THE JOURNAL OF PHYSICAL CHEMISTRY A

ARTICLE

pubs.acs.org/JPCA

Phonon, IR, and Raman Spectra, NMR Parameters, and Elastic Constant Calculations for AlH_3 Polymorphs

P. Vajeeston,* P. Ravindran, and H. Fjellvåg

Center for Materials Science and Nanotechnology, Department of Chemistry, University of Oslo, Box 1033 Blindern N-0315, Oslo, Norway

ABSTRACT:

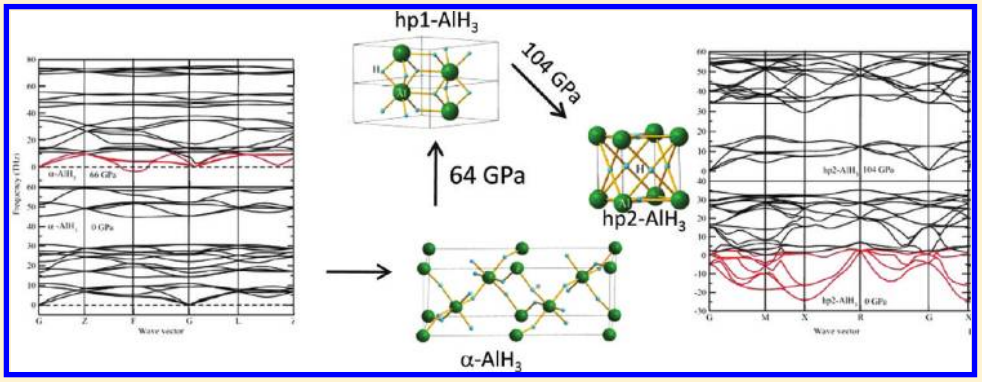

The electronic structure, lattice dynamics, and mechanical properties of AlH_3 phases have been studied by density functional calculations. The chemical bonding in different polymorphs of AlH_3 are evaluated on the basis of electronic structures, charge density analysis, and atomic charges, as well as bond overlap population analysis and the Born effective charges. The phonon dispersion relations and phonon density of states of all the polymorphs of AlH_3 are calculated by direct force-constant method. Application of pressure induces seqauence of phase transitions in β-AlH_3 which are understood from the phonon dispersive curves of the involved phases. The previously predicted phases (*Chem. Mater.* **2008**, *20*, 5997) are found to be dynamically stable. The calculated single crystal elastic constants reveal that all the studied AlH_3 polymorphs are easily compressible. The chemical bonding of these polymorphs have noticeable covalent character (except the *hp*2 phase) according to the present chemical bonding analyses. For all these polymorphs, the NMR-related parameters, such as isotropic chemical shielding, quadrupolar coupling constant, and quadrupolar asymmetry, are also calculated. All IR- and Raman-active phonon frequencies, as well as the corresponding intensities, are calculated for all the AlH_3 polymorphs and are compared with available experimental results.

I. INTRODUCTION

In an approach to a viable hydrogen-based economy, safe, efficient, and affordable ways to store hydrogen is a major challenging issue. Among various hydrogen storage materials currently under investigation, complex hydrides have attracted considerable interest since the discovery by Bogdanovic and Schwickardi that a small amount of $TiCl_3$ doped into $NaAlH_4$ could facilitate accelerated and reversible hydrogen release under moderate conditions.[1,2] Aluminum trihydride (AlH_3) is one of the potential candidate, because it is one of the byproducts in most of the dehydriding reactions in Al-based hydrides. AlH_3 is a unique binary hydride having at least seven crystalline phases (depending upon the synthesis route) with different physical properties and at the same time can store up to 10.1 wt % of hydrogen.[3] Its gravimetric hydrogen density is two times higher than that in liquid hydrogen and much higher than that of most of the known metal hydrides. Thus, AlH_3 is considered as a possible hydrogen storage material.[4] Among the seven polymorphs (α, α', β, γ, δ, ε, and ζ),[5] four (α, α', β, and γ) are experimentally[3,6−8] as well as theoretically[9] characterized, where β-AlH_3 is found to be more stable. Other polymorphs are not yet verified and are formed because of the presence of impurities.[6] One can also stabilize these polymorphs by the application of pressure.[10] The high pressure study by Graetz et al.[11] observed no pressure-induced structural transition in AlH_3 up to at least 7 GPa, which is consistent with earlier high pressure studies.[12,13] Recent high-pressure theoretical[10,14−16] and experimental[17] investigations show that application of pressure transforms α-AlH_3 into two high-pressure phases.[10,17] However, the structure of the *hp*1 phase is not yet solved experimentally.[17] Recently, ref 17 reported that the *hp*1 phase can be either monoclinic or trigonal. On the other hand, recent theoretical investigation by Pickard et al.[16] shows that the *hp*1 phase is in orthorhombic (*Pnma*) structure, but our finding shows that the *hp*1 phase rather has a hexagonal ($P6_3/m$) structure, because this structure of AlH_3 has the lowest energy among all the considered phases at this

Received: February 3, 2011
Revised: August 24, 2011
Published: August 26, 2011

dx.doi.org/10.1021/jp2011342 | *J. Phys. Chem. A* 2011, 115, 10708–10719

pressure range. Further, the orthorhombic (*Pnma*) structure suggested in ref 16 is energetically closer (energy difference is only 0.02 eV/f.u.) to the presently predicted *P*63/*m* structure. Similarly, the electronic structure,[9,18] thermodynamic stability,[19] and dehydriding properties[20] of α-AlH_3 have been well studied. In our previous publication, we have demonstrated that application of pressure makes the sequence of phase transitions from $\beta \rightarrow \alpha' \rightarrow \alpha \rightarrow hp1 \rightarrow hp2$, and the estimated transition pressures are 2.4, 4.3, 64, and 104 GPa, respectively. The coordination of Al has been changed from 6 to 9 in the newly identified high pressure *hp*1 phase and to 12 in *hp*2 polymorph. The calculated electronic structures reveal that α, α', β, and γ polymorphs are nonmetals with calculated band gaps varying between 1.99 and 3.65 eV, whereas the *hp*1 and *hp*2 phases possess semiconducting and metallic behavior, respectively. In this article we have investigated the pressure dependence of lattice dynamical, mechanical, spectroscopic (Raman and IR), and chemical properties of all the above-mentioned AlH_3 polymorphs.

II. COMPUTATIONAL DETAILS

Total energies have been calculated by the projected augmented plane-wave (PAW)[21] implementation of the Vienna ab initio simulation package (VASP).[22] All these calculations were made using the generalized gradient approximation (GGA) exchange correlation functional of Perdew, Burke, and Ernzerhof (PBE)[23] and the projector augmented wave method. It should be noted that both PW91[24] and PBE functionals gave almost the same result. The differences in the energetics and structures from these two functional were found to be negligible, and the results reported here were computed with the PBE functional with Al-h and H-h PAW potentials. Ground-state geometries were determined by minimizing stresses and Hellman-Feynman forces using the conjugate-gradient algorithm with force convergence less than 10^{-3} eV $Å^{-1}$. Brillouin zone integration was performed with a Gaussian broadening of 0.1 eV during all relaxations. From various sets of calculations it was found that 600 **k**-points in the whole Brillouin zone for the α-AlH_3 structure with a 500 eV plane-wave cutoff for basis set are sufficient to ensure optimum accuracy in the computed results. The **k**-points were generated using the Monkhorst-Pack method with a grid size of $10 \times 10 \times 6$ for structural optimization. A similar density of **k**-points and energy cutoff were used to estimate total energy as a function of volume for all the structures considered for the present study. Iterative relaxation of atomic positions was stopped when the change in total energy between successive steps was less than 1 meV/cell. With this criterion, the forces generally acting on the atoms were found to be less than 10^{-3} eV $Å^{-1}$.

The Phonon program developed by Parlinski[25] using direct method was used for lattice dynamic calculations. The force calculations were made using the VASP code with the supercell approach and the resulting data were imported into the Phonon program. Thereafter, the full Hessian was determined and the phonon density of states (DOS) was calculated. The $3 \times 3 \times 3$ supercells were constructed from the optimized structures for the force calculations. The Hessian (harmonic approximation) was determined through a numerical derivative using steps of 0.03 Å in both positive and negative directions of each coordinate to estimate the harmonic potentials. The sampling of the phonon band structure for the calculation of phonon DOS was set to "large" in the Phonon program[25] with a point spacing of 0.005 THz. The Raman and IR spectra for all the polymorphs of AlH_3 are obtained from density functional perturbation theory as implemented in the CASTEP package.[26] For the CASTEP computation we have used the optimized VASP structures with a similar **k**-point mesh as input with Norm-conserving pseudopotentials (energy cut-off 700 eV) and the GGA exchange correlation functional proposed by PBE. Full geometry optimization was made (for the α, α', β, γ, *hp*1, and *hp*2), and we found that both codes gave almost similar lattice parameters and atomic positions.

To gauge the bond strength, we have used the bond overlap population (BOP) values calculated on the basis of the Mulliken population analysis. The density functional perturbation theory with an external electric field was used to calculate the Born effective charges in all the polymorphs of AlH_3 (except for metallic hp2 phase). It has been shown how to calculate NMR chemical shifts in both molecules and solids within DFT and using pseudopotentials to describe the core−valence interactions.[27] The approach is based on gauge including projector augmented waves and is implemented in CASTEP. The single crystal elastic constants and NMR parameters are computed using the CASTEP code along with on the fly pseudopotentials (with energy cutoff 600 eV).[28]

III. RESULTS AND DISCUSSION

At the ambient pressure and zero temperature AlH_3 stabilizes in a β-FeF_3-type atomic arrangement and it has the lowest total energy (β modification). This phase consists of almost regular corner-sharing AlH_6 octahedra with Al−H distances of 1.724 Å (for more details about the structural modifications we recommend the readers to see ref 10). The next energetically favorable phase is orthorhombic β-AlF_3-type (α' modification) atomic arrangement. This structure consists of AlH_6 octahedra where all hydrogen atoms are shared between two octahedra and the calculated average Al−H distance is 1.72 Å. The next energetically favorable structure is α-AlH_3 consisting of corner-shared prefect octahedra which building in a distorted primitive Al sublattice. The Al−H distance at equilibrium is 1.72 Å in this phase also. It is interesting to note that the involved energy difference between the α-, α'- ,β-, and γ-AlH_3 is very small (for more details see ref 10). The required pressure for the β-to-α'-to-α is 2.4 and 4.3 GPa, respectively (see Figures 2 and 3 in ref 10). Further application of pressure shows that the α-modification transforms into $NdOH_3$-derived modification (see Figure 2b in ref 10; *hp*1-AlH_3 modification) around 64 GPa and above 104 GPa a new cubic polymorph (*hp*2-AlH_3 modification) is identified. In these phases, Al coordination is changed from 6 to 9 and 12 for *hp*1 and *hp*2, respectively. The Al−H distances vary within 1.66 to 1.73 Å in *hp*1 and 1.65 Å in *hp*2 phase at the phase transition point.

A. Born Effective Charges and Dielectric Constants. All the studied lattices of AlH_3 belong to the ionic insulating crystals (except *hp*2-AlH_3 polymorphs). For the nonmetallic crystals, the infrared optical modes at the Γ point are normally split into the longitudinal optical (LO) modes and transversal optical (TO) modes and it is often called LO/TO splitting due to the long-range Coulomb interaction (normally caused by the displacement of atoms). The calculated dielectric constants for different polymorphs of AlH_3 are given in Table 2. The Born effective charges (BEC) are obtained from the Berry phase calculations (in VASP code). The BEC give the information about the amount of charge polarized by the application of electric field. The King-Smith and Vanderbilt[30] method was used to calculate

Table 1. Calculated Born-Effective-Charge Tensor Elements (Z) for the Constituents of AlH_3 Polymorphs

	position	*xx*	*yy*	*zz*	*xy*	*xz*	*yx*	*yz*	*zx*	*zy*
NaH										
Na	4*a*	0.95	0.95	0.95	0.0	0.0	0.0	0.0	0.0	0.0
H	4*b*	−0.95	−0.95	−0.95	0.0	0.0	0.0	0.0	0.0	0.0
α-AlH_3										
Z_{Al}	6*b*	2.72 (2.61 ± 0.55[a])	2.72 (2.61 ± 0.55[a])	2.96 (2.81[a])	−0.62	0.0	0.62	0.0	0.0	0.0
Z_H	18*e*	−0.77(−0.62[a])	−1.04 (−0.62[a])	−0.99 (−1.43[a])	−0.23	−0.23	−0.23	−0.39	−0.23	−0.39
α'-AlH_3										
Z_{Al1}	4*a*	2.29	3.17	2.82	0.0	0.0	0.0	0.51	0.0	−0.55
Z_{Al2}	8*f*	3.02	2.50	2.85	0.45	0.30	0.52	−0.44	−0.22	0.29
Z_{H1}	8*f*	−1.62	−0.55	−0.63	0.0	0.0	0.0	−0.04	0.0	0.05
Z_{H2}	16*h*	−0.82	−1.31	−0.62	0.46	0.00	0.45	−0.02	−0.03	0.02
Z_{H3}	4*c*	−0.51	−0.73	−1.60	0.0	0.0	0.0	0.0	0.0	0.0
Z_{H4}	8*h*	−0.65	−0.56	−1.59	−0.07	0.0	−0.09	0.0	0.0	0.0
β-AlH_3										
Z_{Al}	16*d*	2.72	2.72	2.72	0.37	0.37	0.37	0.37	0.37	0.37
Z_H	48*f*	−0.59	−1.07	−1.07	0.0	0.0	0.0	−0.55	0.0	−0.55
γ-AlH_3										
Z_{Al1}	2*b*	2.41	3.20	3.23	0.72	0.0	0.42	0.0	0.0	0.0
Z_{Al2}	4*g*	2.90	2.21	2.75	0.33	0.0	0.37	0.0	0.0	0.0
Z_{H1}	2*d*	−1.81	−0.69	−0.59	−0.46	0.0	−0.40	0.0	0.0	0.0
Z_{H2}	4*g*	−0.98	−0.66	−0.58	−0.16	0.0	−0.26	0.0	0.0	0.0
Z_{H3}	4*g*	−0.82	−1.59	−0.64	0.66	0.0	0.50	0.0	0.0	0.0
Z_{H4}	8*h*	−0.70	−0.61	−1.42	0.06	0.32	0.07	−0.14	0.32	−0.17
*hp*1-AlH_3										
Z_{Al}	2*d*	2.67	2.67	2.97	−0.01	0.0	0.01	0.0	0.0	0.0
Z_H	6*h*	−1.16	−0.62	−0.99	−0.01	0.0	−0.02	0.0	0.0	0.0

[a] Calculated value from ref 19.

Table 2. Components of the High- and Low-Frequency Dielectric Constant Tensor ε and Calculated Zero-Point Energy (ZPE; eV/f.u.) for AlH_3 Polymorphs

	α	α'	β	γ	*hp*1 (tp)	*hp*2 (tp)
$\varepsilon^{\infty}_{xx}$	4.75 (4.25[a]; 4.8[b])	4.25	3.94	4.42	8.49	
$\varepsilon^{\infty}_{yy}$	4.75 (4.8[b])	4.19	3.94	4.14	8.49	
$\varepsilon^{\infty}_{zz}$	4.94 (4.9[b])	4.36	3.94	4.60	8.99	
ε^{0}_{xx}	13.19 (10[b])	11.26	9.06	10.72	13.74	
ε^{0}_{yy}	13.19 (10[b])	10.86	9.06	11.98	13.74	
ε^{0}_{zz}	15.62 (14.3[b])	12.6	9.06	12.07	18.49	
ZPE	0.661 (0.660[c], 0.644[b])	0.663 (0.662[c])	0.664 (0.666[c])	0.655	0.887	0.955

[a] Measured average value from ref 40. [b] Calculated value from ref 19. [c] Calculated value from ref 9.

the polarizations in the perturbed cells and subsequently the BEC tensor elements for the ions involved and the calculated BEC are tabulated in Table 1. Our calculated BEC value for the α phase is in agreement with the literature value.[19] It should be noted that BEC tensor affects only the LO modes at the Γ point (more discussion about this topic can be found in refs 25 and 31−35). The possible other application of BEC analysis is to evaluate bonding characteristics of materials.[36] For example, in NaH case the diagonal components of the effective charges in a Cartesian frame satisfy the relation $Z_{xx} = Z_{yy} = Z_{zz}$, whereas the off-diagonal components turn out to be negligible. This is as expected for ionic compounds due to the spherical character of charge distribution in ionic bonds. For α- and *hp*1-AlH_3 polymorphs the diagonal components of the effective charges at the Al sites are almost equal ($Z_{xx} \approx Z_{yy} \approx Z_{zz}$). Some of the off-diagonal components for the *hp*1 phase are very small but finite. Because of the higher symmetry structure for the β modification, all the components of the calculated BEC in the diagonal and off-diagonal parts at the Al site are equal. On the other hand, for the H site, the calculated diagonal component of the BEC is not symmetric ($Z_{xx} = Z_{yy} \neq Z_{zz}$). The off-diagonal components are also not symmetric and have higher values. The calculated BEC

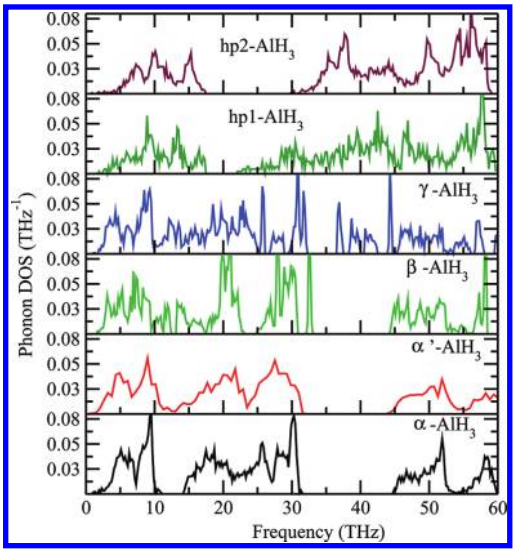

Figure 1. Calculated total phonon density of states for AlH_3 in different polymorphs. The modifications are noted in the corresponding panel.

values for the α'- and γ-AlH_3 polymorphs are having almost similar features in the diagonal components and off-diagonal components. In general, for pure ionic systems, the calculated average BEC will be same as that of the nominal ionic charge. But, for all the studied AlH_3 polymorphs, the calculated average BEC values clearly show that the bonding interaction deviates from pure ionic case. Hence, the "average BEC charges" are deviating from the nominal ionic charges (3 for Al and −1 for H). Further, the present study predicts that the BEC values are highly directional dependent for both Al (except in β modification) and H sites in the AlH_3 polymorphs indicating the presence of finite covalent interaction. It should be noted that a similar behavior was observed in $NaAlH_4$ and Na_3AlH_6 systems.[9,37]

The components of the high- and low-frequency dielectric constant tensor, ε, were calculated, including local field effects, using the linear response method, as implemented in the CASTEP code, and are listed in Table 2. Our calculated ε for the α phase is in very good agreement with the available literature value.[19] There are no experimental measurements for the AlH_3 polymorphs (except α polymorph) available for comparison. Hence, we have computed the ε for LiH to cross check the reliability of our calculated values with the available experimental result. For LiH, our calculated ε value (3.31) is in excellent agreement with the experimental value of 3.61.[38] The ε value obtained from the present calculation using screened exchange with LDA correlation (sX-LDA) with Ceperley and Alder functional (using CASTEP code) is found to be much better than the other GGA and LDA values reported in the literature for the LiH phase.[39] The corresponding value using the linear response method for the LiH is 3.29. For the α polymorph the measured dielectric constant at room temperature is 4.25.[40] The calculated (using linear response method) average ε value of 4.39 is found to be in very good agreement with the corresponding experimental finding. From the good agreement of our calculated dielectric constants for LiH and α-AlH_3 with available experimental values, we conclude that the predicted ε values for the remaining AlH_3 polymorphs (given in Table 2) are expected to be reliable.

B. Phonon Dispersion Relations and Phonon Density of States. The total phonon density of states (PDOS) are calculated at the equilibrium volumes for α, α', β, and γ phases of AlH_3. On the other hand, for the *hp*1 and *hp*2 modifications, the PDOS are calculated at equilibrium as well as at the phase transition point. The calculated PDOS of AlH_3 polymorphs are displayed in Figure 1. For all these polymorphs, no imaginary frequency was observed, indicating that all the structures are stable or at least they are dynamically stable. Hence, the predicted phases are stable at the corresponding pressures. It is interesting to note that the involved energy difference between the α-, α'-, β-, and γ-AlH_3 phases are very small and, hence, one can easily modify one polymorph into another by application of temperature or pressure. This is one of the reasons why depending upon the synthesis route or conditions it is possible to stabilize different polymorphs of AlH_3.[5−8] α-, α'-, β-, and γ-AlH_3 have almost the same phonon density of states. Similarly, the remaining phases *hp*1 and *hp*2 also have almost similar phonon density of states (DOS). Hence, we have displayed in Figure 2 only the partial phonon DOS for α-, *hp*1-, and *hp*2-AlH_3 polymorphs. In the studied cases, the partial phonon DOS is plotted along three directions *x*, *y*, and *z*. For Al atoms, the vibrational modes along the *x*, *y*, and *z* directions are almost identical. Similarly, for the H atoms, the vibrational modes along the *x*, *y*, and *z* directions are almost identical (except for *hp*1 phase). In the *hp*1 phase, the modes along the *y* in the H site is slightly different from those of the *x* and *z* directions (see Figure 2a). Because the mass of H atom is much smaller than that of Al atom, Figure 1 shows that for the *hp*1 and *hp*2 phases the high frequency modes above 20 THz are dominated by H atom, and in α-phase, the corresponding frequencies are around 10 THz. The low frequency modes below 20 THz in *hp*1 and *hp*2 phases are mainly dominated by Al, and for the α-phase, the Al modes are present below 10 THz.

The calculated phonon dispersion curves along the high symmetry direction of the Brillouin zone for the polymorphs (α-, α'-, β-, and γ-AlH_3) are plotted for their equilibrium volume, and from these it is clear that they do not have any soft modes (due to the space limitation the phonon dispersive curve for α-AlH_3 phase is only presented; see Figure 3). On the other hand, for the *hp*1 and *hp*2 polymorphs, the calculated phonon dispersion curves at equilibrium volume have negative modes (see Figures 4 and 5). This indicates that, at least at the equilibrium condition, the *hp*1 and *hp*2 polymorphs are dynamically unstable. Application of pressure transforms the α-AlH_3 phase into the *hp*1 polymorphs at 64 GPa. It should be noted that, even though the phase transition takes place at 64 GPa, it is hard to see the phonon soft modes. Hence, we have displayed the phonon spectra and phonon DOS at 66 GPa in Figure 4. At 66 GPa, the calculated phonon dispersion curves along the high symmetry directions for the equilibrium polymorphs show the presence of soft modes (see Figure 3). On the other hand, in the *hp*1 phase, the soft phonon modes disappears and this phase becomes dynamically stable in this pressure range (see Figure 4). If the pressure exceeds 104 GPa, the *hp*1 phase becomes dynamically unstable, whereas dynamically unstable *hp*2 phase becomes dynamically stable (see Figure 5). This finding is consistent with the conclusion arrived in our previous publication[10] where the results are obtained from total energy calculations and the transition pressures agree very well with the experimental observations.[17] It may be noted that, in ref 17, it is reported that the *hp*1 phase can be either monoclinic or trigonal. On the other hand, recent theoretical investigation by Pickard et al.[16] shows that the *hp*1 phase is orthorhombic (*Pnma*). But our finding

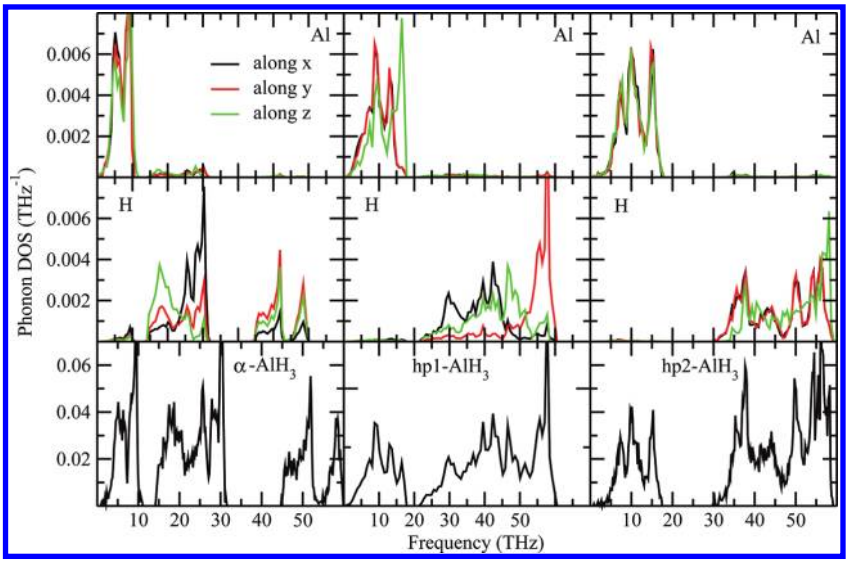

Figure 2. Calculated partial phonon density of states for α-, *hp*1-, and *hp*2-AlH_3 polymorphs. The modifications are noted in the corresponding panel and the phonon mode along different directions are marked with different color.

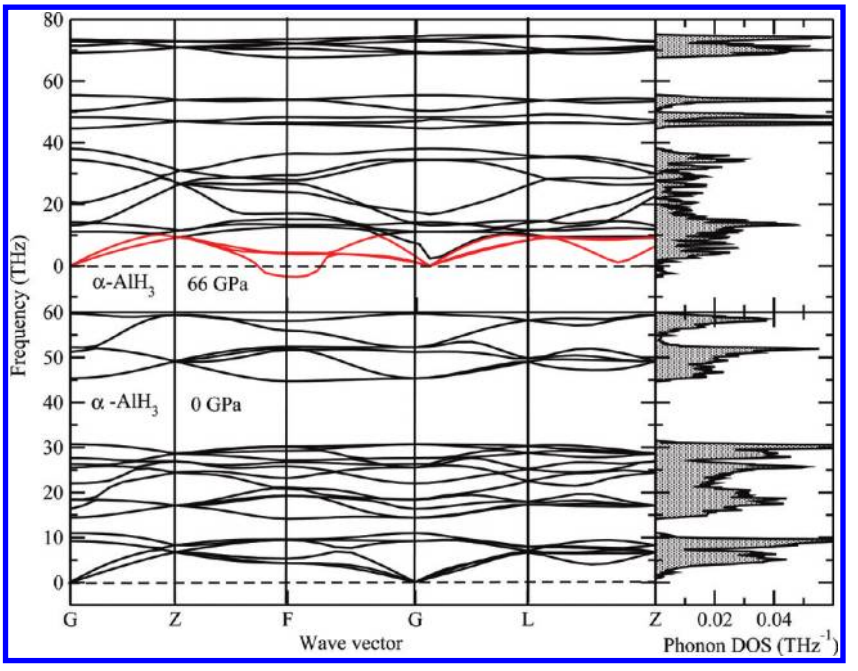

Figure 3. Calculated phonon spectra for the α-AlH_3 phase at equilibrium volume (lower panel), above the phase transition point (at 66 GPa; upper panel), and the corresponding phonon DOS are given in the right-hand side of the figure. The negative frequency values correspond to the imaginary scale as $(-\omega^2)^{1/2}$ and are marked by red color.

shows that the *hp*1 phase rather has a hexagonal ($P63/m$) structure, which is dynamically stable within this pressure range.

The phonon frequencies at the Γ point for the AlH_3 polymorphs are summarized in Table 3. According to the symmetry analysis (crystal point group), the optical modes at the Γ point can be classified into the following symmetry species for different polymorphs of AlH_3:

$$\Gamma_\alpha = A_{1g}(R) + 3E_g(R) + 2A_{2u}(I) + 4E_u(I) \quad (1)$$

$$\Gamma_{\alpha'} = 8A_g(R) + 7B_{1g}(R) + 5B_{2g}(R) + 7B_{3g}(R) + 11B_{1u}(I) + 12B_{2u}(I) + 10B_{3u}(I) \quad (2)$$

$$\Gamma_\beta = A1_g(R) + Eg(R) + 3T2g(R) + 4Tiu(I) \quad (3)$$

$$\Gamma_\gamma = 9A_g(R) + 9B_{1g}(R) + 6B_{2g}(R) + 6B_{3g}(R) + 7B_{1u}(I) + 12B_{2u}(I) + 12B_{3u}(I) \quad (4)$$

$$\Gamma_{hp1} = 2A_g(R) + E_{1g}(R) + 3E_{2g}(R) + A_u(I) + 2E_{1u}(I) \quad (5)$$

$$\Gamma_{hp2} = E_g(R) + T_{2g}(R) + 2T_{1u}(I) \quad (6)$$

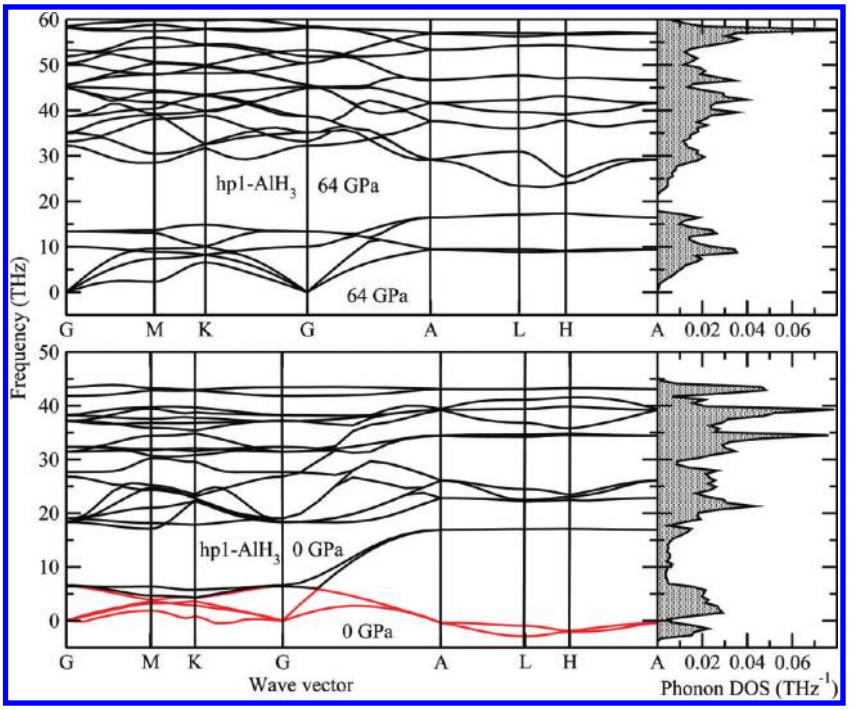

Figure 4. Calculated phonon spectra for the *hp*1-AlH_3 modification at equilibrium volume (lower panel), at the phase transition point (upper panel), and the corresponding phonon DOS are given in the right-hand side of the figure. The negative phonon frequency values correspond to the imaginary scale as $(-\omega^2)^{1/2}$ and are marked by red color.

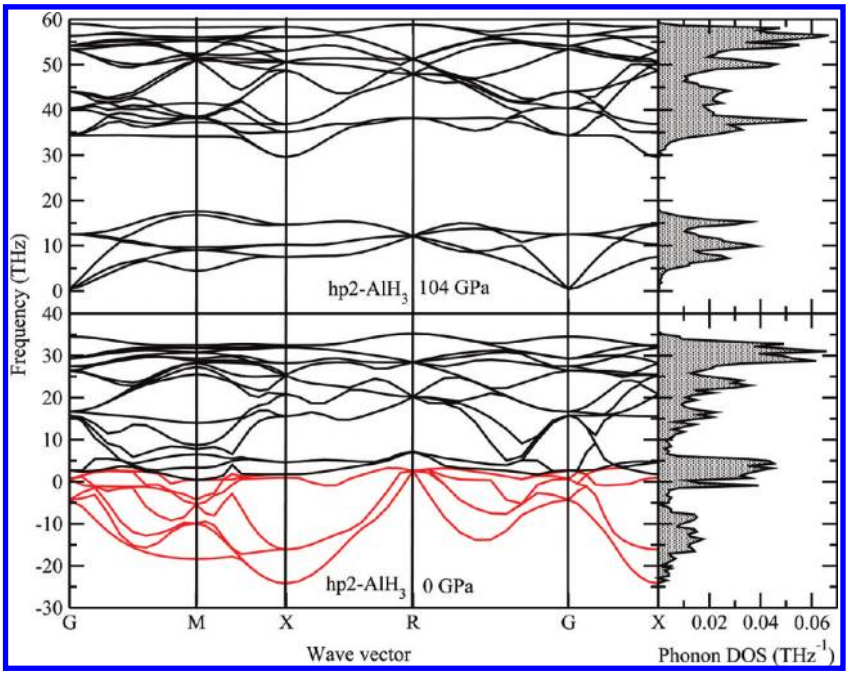

Figure 5. Calculated phonon spectra for the *hp*2-AlH_3 modification at zero pressure (lower panel), at the phase transition point (upper panel), and the corresponding phonon DOS are given in the right-hand side of the figure. The negative frequency values correspond to the imaginary scale as $(-\omega^2)^{1/2}$ and are marked by red color.

where the notations of *R* and *I* refer to Raman active and infrared active modes, respectively. The calculated Raman modes for the α phase are in good agreement with the corresponding experimental[41] as well as other theoretical findings.[19] The deviation between the present study and Wolverton et al.[19] is due to the difference in the computation. The bulk experimental structural parameters are used in ref 19 with LDA and linear-response calculations for zone-center phonon frequencies, whereas we have used fully optimized theoretical structural parameters. It may be noted that the calculated Raman frequencies using direct

Table 3. Calculated Frequency (in cm^{-1}) for the Modes at the Γ Point of the Brillouin Zone for AlH_3 Polymorphs at Equilibrium Volume[a]

	α-AlH_3	α'-AlH_3	β-AlH_3	γ-AlH_3	$hp1$-AlH_3	$hp2$-AlH_3
Raman						
	A_{1g}: 698.59 (812[b], 723[c]); Eg: 464.79 (490[b]; 512[c]), 1003.52 (993[b],1043[c]), 1416.56 (1481[b], 1501[c]), 1416.56 (1481[b], 1501[c])	A_g: 387, 475, 733, 789, 940, 968, 1037, 1862; B_{1g}: 284, 655, 745, 842, 974, 1384, 1875; B_{2g}: 613, 872, 1446, 1459, 1950; B_{3g}: 654, 748, 806, 1013, 1456, 1835, 1940	A_{1g}: 1100; E_g: 818; T_{2g}: 713, 1002, 1882	A_g: 246, 419, 524, 785, 1028, 1269, 1457, 1497, 1901; B_{1g}: 280, 440, 510, 766, 1052, 1289, 1456, 1773, 1848; B_{2g}: 251, 482, 680, 846, 944, 1526; B_{3g}: 228, 291, 721, 869, 943, 1533	A_g: 1487, 1725; E_{1g}: 1484; E_{2g}: 446, 1225, 1977	E_g: 1931; T_{2g}: 1833
Infrared						
	A_{2u}: 529, 1652; E_u: 293, 615, 818, 1681	B_{1u}: 142, 162, 290, 364, 552, 649, 847, 933, 1637, 1688, 1698; B_{2u}: 282, 313, 324, 341, 657, 711, 777, 845, 917, 952, 998, 1640; B_{3u}: 155, 281, 321, 588, 692, 735, 854, 933, 1642, 1749	T_{1u}: 311, 709, 899, 1582	B_{1u}: 321, 484, 560, 696, 732, 1018, 1585; B_{2u}: 129, 207, 312, 544, 558, 696, 956, 1179, 1339, 1577, 1673, 1951; B_{3u}: 156, 226, 277, 497, 652, 782, 964, 1188, 1329, 1596, 1636, 1952	A_u: 975; E_{1u}: 1096, 1680,	T_{1u}: 1116, 1362

[a] For the $hp1$ and $hp2$ phases, the modes are calculated at the phase transition point (i.e., 64 and 104 GPa, respectively). [b] Theoretical values from ref 19. [c] Experimentally observed values from ref 41.

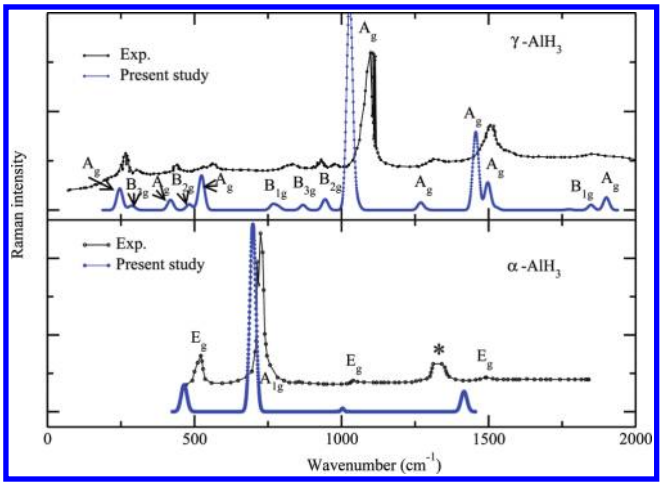

Figure 6. Theoretically simulated and experimentally[41] observed Raman spectra for the α- and γ-AlH_3 modifications at ambient conditions. For more clarity, only selected Raman active modes are marked in the γ-AlH_3 Raman spectra. In the experimental spectra, symbol "*" denotes the Raman signal from diamond.

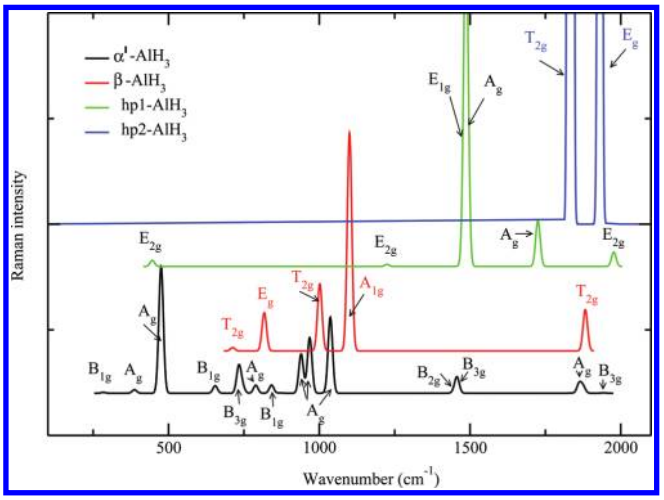

Figure 7. Theoretically simulated Raman spectra for the α', β, $hp1$-, and $hp2$-AlH_3 modifications at ambient conditions.

method for $NaAlH_4$ are found to be in good agreement with the corresponding experimental values within 5% error.[9] In general, the calculated Raman active phonon frequency values are underestimated compared with corresponding experimental frequencies. We have displayed the simulated and experimentally obtained Raman spectra for α- and γ-AlH_3 in Figure 6. The calculated overall peak positions and intensities for the α- and γ-AlH_3 phases agree well with the corresponding experimental spectra. For the γ-phase, quite a large number of low-intensity signals are visible in the Raman spectrum. To have clarity in the Raman spectrum, we have marked only a limited number of peaks in Figure 6, and all the values are tabulated in Table 3. Moreover, to understand the origin of Raman peaks experimentally, it is important to compare it with the theoretical spectra where one can obtain information about the active modes for a specific structural arrangement. Due to experimental limitations and metastability, it is difficult to obtain pure form of α' and β phases

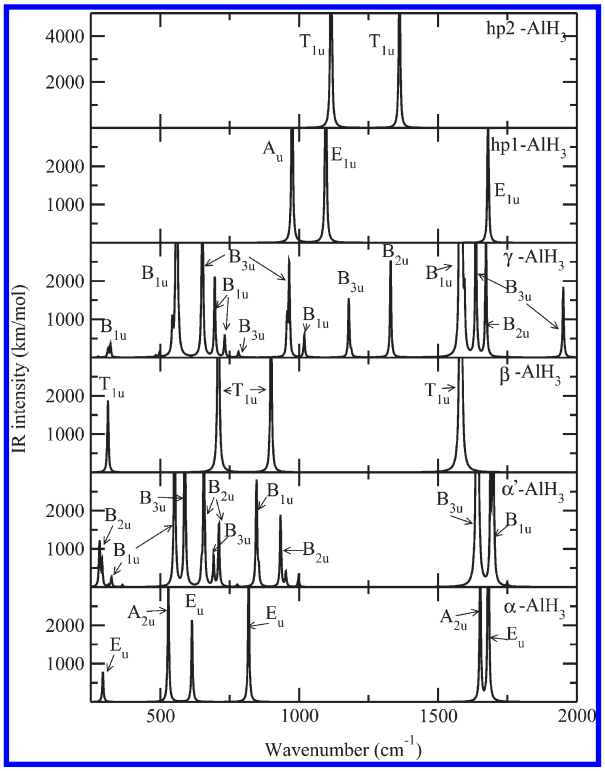

Figure 8. Theoretically simulated IR spectra for the α-, α'-, β-, γ-AlH_3 modifications at ambient conditions. For the *hp*1 and *hp*2 phases, the spectra are simulated at the phase transition point (64 and 104 GPa, respectively). For more clarity, only selected IR active modes are marked in the α'- and γ-AlH_3 IR spectra.

at ambient conditions. The sample mostly contains more than one phases, and in such situations we can use the theoretically simulated spectra to distinguish the different phases. For this reason, we have simulated Raman and IR spectra for all these studied phases, which are displayed in Figures 6−8.

The calculated zero-point energy (ZPE) for the AlH_3 polymorphs varies from 0.655 to 0.955 eV/f.u. (see Table 2). Among the studied phases, the γ phase has minimum ZPE value and *hp*2 has maximum value. Our calculated ZPE for the AlH_3 (0.661 eV/f.u.) is in good agreement with the literature values (0.660 and 0.644 eV/f.u.; refs 9 and 19). Similarly, our calculated ZPE for the α' and γ phases are in good agreement with the previous calculations.[9] However, the calculated ZPE for the ambient phases (α, α', β, and γ) are very close to each other. This finding suggests that the exclusion of the temperature effect may not affect our conclusion regarding the transition pressures reported in our previous study[10] considerably. On the other hand, for the high pressure phases, the ZPE values are much higher than the ambient phases and this may be the possible reason why the theoretical predictions always gives higher transition pressure. The other possible reason is that in all our theoretical simulation we have assumed phase pure sample with ideal structure where the temperature effect is not included. But, in the real case, the sample is burdened with impurities, defects, and presence of more than one phase. This might make considerable difference in the phase transition pressure. Also, the exchange correlation functional used in the present study may not be sufficient to predict the transition pressures correctly.

Table 4. Mulliken Population Analysis for AlH_3 Polymorphs and the Bond Overlap Population (between Al and H) is Denoted as BOP[a]

polymoph	atom	MEC	BOP	HSE
α-AlH_3	Al	1.24	0.35	1.22
	H	−0.41		
α'-AlH_3	Al	1.24 to 1.26	0.51 to 0.52	1.38 to 1.41
	H	−0.41 to −0.43		
β-AlH_3	Al	1.23	0.5	1.39
	H	−0.41		
γ-AlH_3	Al	1.12 to 1.24	0.42 to 0.52	1.05 to 1.37
	H	0.28 to 0.5		
*hp*1-AlH_3 (eq)	Al	0.89	0.91	0.29
	H	−0.28		
*hp*1-AlH_3 (tp)	Al	1.02	1.08	0.52
	H	−0.33		
*hp*2-AlH_3 (eq)	Al	0.83	0.30	−1.75
	H	−0.28		
*hp*2-AlH_3 (tp)	Al	1.33	0.24	0.45
	H	−0.44		

[a] The Mulliken-effective charges (MEC) are given in terms of *e* and the hydrogen site energy (HSE) is given in terms of eV.

IV. CHEMICAL BONDING

From the simple chemical point of view, the interaction between Al and H in AlH_3 is either covalent (sharing of electrons) or ionic (Al donate electron to H). According to BEC analysis, the bonding interaction is not purely ionic in AlH_3 polymorphs (except hp2 phase). But, from our experience on this type of hydride, we found that the evaluation of the chemical bonding in materials becomes difficult when the number of constituents increases.[37] In an attempt to quantify the bonding and estimate the amount of electrons on and between the participating atoms, we have made Mulliken-population analysis. Although there is no unique definition to identify how many electrons are associated with an atom in a molecule or an atomic grouping in a solid, it has nevertheless proved useful in many cases to perform population analyses. Due to its simplicity, the Mulliken population[42] scheme has become the most popular approach. However, this method is more qualitative than quantitative, providing results that are sensitive to the atomic basis. The calculated Mulliken charges are reported in Table 4 for AlH_3 polymorphs. The commonly recognized nearly pure ionic compound LiH gave Mulliken effective charges (MEC) of +0.98*e* for Li and −0.98*e* for H. The overlap populations between Li^+ and H^- in LiH is close to zero, as expected for ionic compounds. In all the equilibrium phases of AlH_3 (i.e., α, α', β, and γ modifications), Al always gives 1.12−1.24 electrons to H sites, and each H gets around 0.28−0.5 electrons. For the high pressure phases of AlH_3 (*hp*1 and *hp*2 at their equilibrium), Al always gives 0.83−0.89 electrons to H sites and each H gets 0.28−0.3 electrons from the Al site. These values are smaller than that in equilibrium structures of other polymorphs. At the transition point of *hp*1 and *hp*2 phases, the calculated MEC have similar values like other polymorphs, that is, Al donates around 1.02−1.33 *e* to the H sites. These values are much smaller than that from pure ionic picture (+3 for Al and −1 for H).

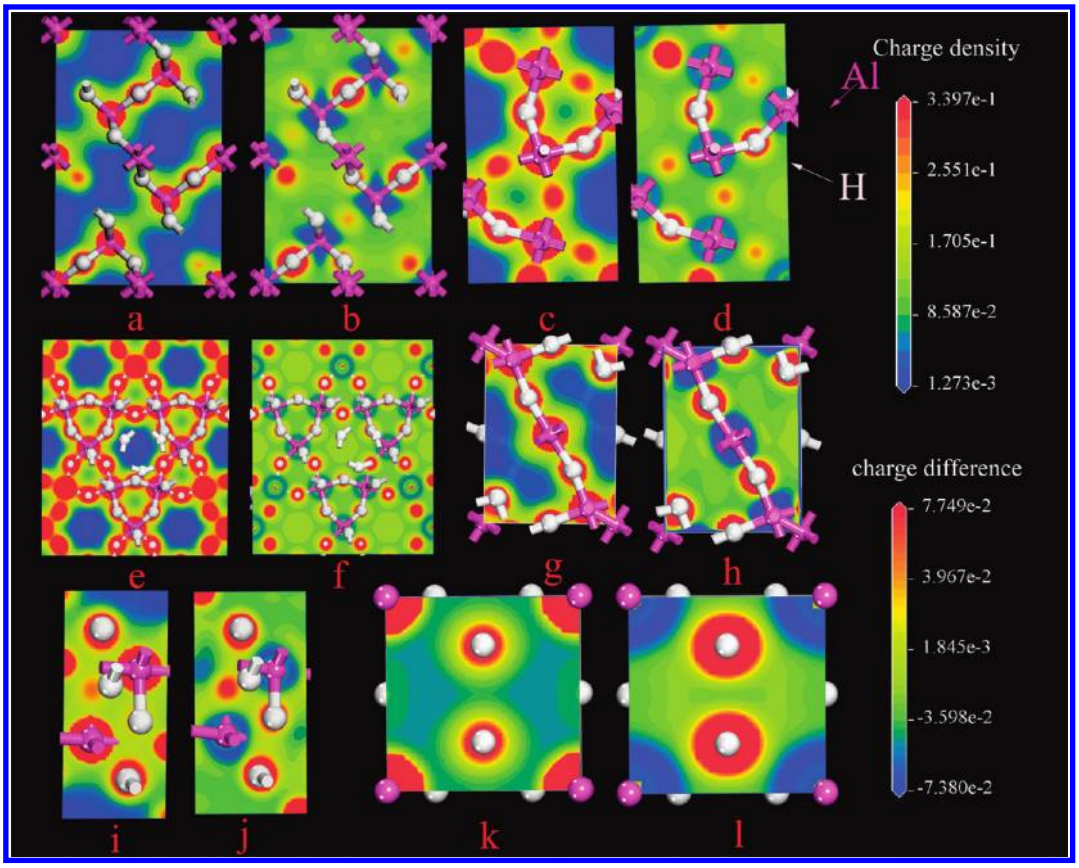

Figure 9. Calculated valence electron charge density distribution (a, c, e, g, i, and k) and charge transfer (b, d, f, h, j, and l) plot for α-, α'-, β-, γ-, *hp*1-, and *hp*2-AlH_3 polymorphs.

To gain more information about the bonding situation in the AlH_3 polymorphs, we turned our attention to charge-density analysis. The α, α', β, and γ modifications of AlH_3 exhibit a similar features see Figure 9a, c, e, g, i, and k. According to the charge-density distribution at the Al and H sites, it is evident that the highest charge density resides in the immediate vicinity of the nuclei. The nonspherical charge distribution around Al and H clearly indicates that the bonding between Al and H has noticeable covalent character. This can be expected according to the electronegativities of the constituents (for Al 1.61 and H 2.20, from the Linus Pauling's scale) that the bonding in these polymorphs should have a dominant covalent character. The main difference between the bonding in equilibrium phases (α, α', β, and γ modifications) and *hp*2 is the formation of metallic bonds. As a result, the charge density distribution in *hp*2 is almost identical in all direction of the crystal (Figure 9f). The bonding behavior in the *hp*1 phase is between that of α and *hp*2 phases and it has mixed bonding character (see Figure 9d). From the charge transfer plot (the difference between the electron density of the compound and the electron density of the constituent atoms), one can obtain insight on redistribution of electrons when the solid is formed. This allows one to see how the actual chemical bond is formed in real space. To depict the role of charge transfer, we have displayed the charge transfer plot for α, α', β, γ, *hp*1, and *hp*2 in Figure 9b, d, f, h, j, and l, respectively. From Figure 9 it is clear that electrons are transferred from Al to the H site. So, there is considerable ionic bonding component present between Al and H. Due to the presence of considerable covalent bonding, the charge depletion at the Al site is not spherically symmetric (see Figure.9b).

Further understanding about the interaction between the constituents can be obtained from the bond overlap population (BOP) values calculated on the basis of the Mulliken population analysis. The BOP can provide useful information about the hybridization interaction between constituents. A high BOP value indicates a strong covalent bond, while a low BOP value indicates an ionic interaction. To use AlH_3 as a hydrogen storage material one must weaken the Al−H bond. The calculated BOP values for the Al−H in different polymorphs are displayed in Table 4. The BOP values for the Al−H bonds among the six polymorphs at their equilibrium given in Table 4 vary between 0.30 and 0.91 (minimum in *hp*2 phase and maximum in *hp*1 phase). This is consistent with the general expectation of loss of covalency with pressure. At the phase transition point, the calculated BOP varies from 0.24 and 1.08 for *hp*1 and *hp*2, respectively. The high pressure *hp*2 phase has smaller BOP value than the rest of the polymorphs and also it has metallic character. This means that the *hp*1 polymorph is a potential candidate for the hydrogen storage application compared with other polymorphs.

To substantiate this observation, we have calculated the H site energy (HSE; ΔE) in these polymorphs. The H site energy is calculated in the following manner $\Delta E = (E_{H_{vac}} + 1/2E_{H_{mol}}) - E_{solid}$, where $E_{H_{vac}}$ and E_{solid} refers to the energy of the system with and without H vacancy, $E_{H_{mol}}$ is the total energy of a free H_2 molecule calculated in a large box. The calculated HSE for α, α', β, and γ modifications shows that all these phases have almost a

similar value. On the other hand, the equilibrium *hp*1-AlH_3 phase has much lower HSE value than that in α, α', β, and γ polymorphs. This implies that the removal of hydrogen from the *hp*1 phase is much easier than from other polymorphs and such high pressure phases may be stabilized by chemical substitution. The lowering of HSE along with the formation of metallic bond should lead to very favorable kinetic conditions in the hydrogen desorption process. If one considers the *hp*2-phase, the calculated HSE value at the ambient pressure is negative. This indicates that *hp*2 will not be stable at ambient conditions and it will instantaneously decompose in to Al and H. But, at the phase transition point, the calculated HSE value for *hp*2 phase is 0.45 eV, indicating that it will be stable at high pressures.

V. MECHANICAL PROPERTIES

The elastic constants of a material describe its response to an applied stress or, conversely, the stress required to maintain a given deformation. Both stress and strain have three tensile and three shear components, giving six components in total. The linear elastic constants form a 6×6 symmetric matrix, having 27 different components, such that $\sigma_i = C_{ij}\varepsilon_j$ for small stresses, σ, and strains, ε.[43] Any symmetry present in the structure may make some of these components equal and others may be fixed at zero. Thus, a cubic crystal has only three different symmetry elements (C_{11}, C_{12}, and C_{44}), each of which represents three equal elastic constants ($C_{11} = C_{22} = C_{33}$; $C_{12} = C_{23} = C_{31}$; $C_{44} = C_{55} = C_{66}$). A single strain with nonzero first and fourth components can give stresses relating to all three of these coefficients, yielding a very efficient method for obtaining elastic constants for the cubic system.[44] The calculation of elastic constants from first principles usually involve setting either the stress or the strain to a finite value, reoptimizing any free parameter and calculating the other property (the strain or stress, respectively). By the careful selection of the applied deformation within the elastic limit, the elastic constants can be determined. However, applying a given homogeneous deformation (strain) and calculating the resulting stress usually requires less computational effort, because the unit cell is fixed and does not require optimization. Hence, we used this finite strain technique to calculate the elastic constants. From the calculated C_{ij} values one can calculate the mechanical properties such as the bulk modulus (response to an isotropic compression), Poisson coefficient, Lame constants, and so on.

The finite strain technique has been successfully used to study the elastic properties of a range of materials.[45−50] These studies clearly indicate that the accuracy of DFT elastic constants is typically within 10% or less of experiment.[51] This means that one can predict the elastic constants reliably for new materials or for materials where experimental data do not exist. If we compare the availability of elastic constants for hydrides with that of intermetallics as well as oxides, the mechanical property studies are very limited for hydrides both theoretically as well as experimentally. The calculated elastic constants for AlH_3 polymorphs at their equilibrium volume are listed in Table 5. This table indicates that the α-AlH_3 phase is stiffest along the *c* axis because its C_{33} value exceeds those for the other polymorphs. In contrast, α'-AlH_3 and γ-AlH_3 are stiffest along the *a* and *c* axes, as suggested by their higher C_{11} and C_{22} values. The derived bulk modulus (B_0) values from the elastic constants vary between 24 and 35 GPa for the different polymorphs of AlH_3. Compared with intermetallic-based hydrides, these AlH_3 polymorphs have low B_0 values, implying that they are easily compressible.

Table 5. Calculated Elastic Constants C_{ij} (GPa), Bulk Modulus B_0(GPa), and Compressibility (GPa^{-1}) at Zero Pressure for α-, α'-, β-, and γ-AlH_3[a]

C_{ij}	α	α'	β	γ	*hp*1	*hp*2
C_{11}	71.82	100.50	74.20	93.93	320.80	863.06
C_{12}	0.99	18.41	16.54	34.90	213.37	246.30
C_{13}	13.94	−6.02		7.00	287.55	
C_{14}	9.78					
C_{22}		82.56		84.85		
C_{23}		−21.15		8.08		
C_{33}	120.78	97.99		119.44	423.82	
C_{44}	58.63	31.16	38.19	24.46	198.08	182.22
C_{55}		29.74		29.33		
C_{66}		44.o1		34.86		
B_0	32.5	28.00	35.76	44	269	452
Com	0.031	0.036	0.035	0.022	0.004	0.002

[a] For the *hp*1 and *hp*2 polymorphs these values are calculated at the phase transition point.

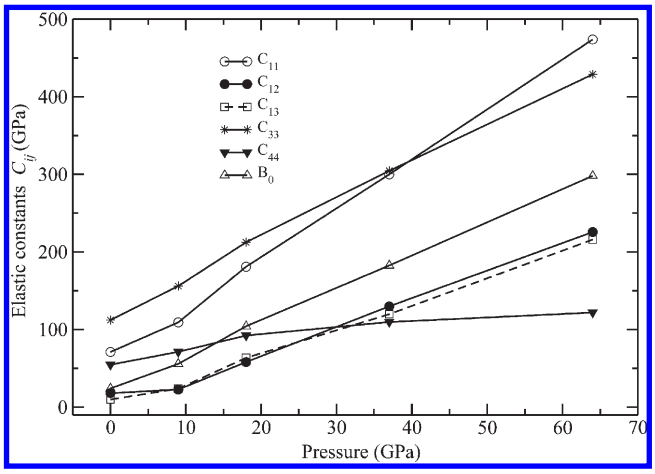

Figure 10. Calculated elastic constants C_{ij} and the bulk modulus B_0 variation as a function of pressures for the α-AlH_3 polymorph.

It is worthy to note that, for the α phase, the experimentally derived B_0 value varies between 42 and 49 ± 4 GPa.[11,12,17] The theoretical values presented in ref 11 are found to be closer to the experimental value. However, our theoretical study shows that, even though the calculated equilibrium volumes are very closer to the experimental and other theoretical values, the calculated B_0 value is almost half. This finding is consistent with our previous study, where the B_0 value was estimated from our total energy versus volume curve. An independent high pressure measurement for high quality samples at low temperature is recommended to clarify this discrepancy.

The variations in the elastic constants with pressure for α-AlH_3 are shown in Figure 10. It is clear that C_{11}, C_{12}, C_{13}, and C_{33} exhibit linearly increasing trends with pressure for all the polymorphs of AlH_3. On the other hand, C_{44} increases monotonically up to 20 GPa and afterward it becomes constant up to 64 GPa with positive value always. This leads us to conclude that the α-phase of AlH_3 is mechanically stable up to 64 GPa.

Table 6. Computed Isotropic Chemical Shielding (σ_{iso}; in ppm), Quadrupolar Coupling Constant (C_Q; in MHz), and Quadrupolar Asymmetry (η_Q) for AlH_3 Polymorphs

parameter	element	α	α'	β	γ	$hp1$
σ_{iso} (ppm)	Al1	559.46	546.29	528.07	515.32	592.60
	Al2		541.29		542.88	
C_Q (MHz)	Al2	0.17 (0.25[a])	0.453	0.475	3.88 (4.2[a])	7.186
	Al2		0.121		2.74 (2.9[a])	
η_Q	Al1	0.05 (0.1[a])	0.29	0.05	0.27 (0.3[a])	0.06
	Al2		0.61		0.41 (0.55[a])	

[a] Experimental value from ref 52.

VI. CALCULATION OF NMR PARAMETERS

NMR is often used as an analytical tool to aid structure prediction. Knowledge about the crystal structures is a prerequisite for the rational understanding of the solid-state properties of new materials. The relative complexity of crystal structures in multicomponent materials makes structure determination is a challenging task. Even though the general features of the crystal structure are understood often, a detailed analysis of the geometry proves elusive. When NMR parameter calculations are used, it is possible to simulate the NMR spectrum for a series of related structures until a match is discovered between the computed and experimental results. In this way, theory complements experiment and contributes to the determination of the correct crystal structure.

In this connection we have calculated the isotropic chemical shielding (σ_{iso}), quadrupolar coupling constant (C_Q), and quadrupolar asymmetry parameter (η_Q) for different polymorphs of AlH_3 (except $hp2$ phase) using the following relations.

$$\sigma_{iso} = (\sigma_{xx} + \sigma_{yy} + \sigma_{zz})/3 \quad (7)$$

$$C_Q = eQV_{zz}/h \quad (8)$$

$$\eta_Q = (V_{xx} - V_{yy})/V_{zz} \quad (9)$$

where σ refers to the chemical shielding tensor in the principal axis frame. This is an absolute value of the isotropic chemical shielding and not relative to any standard. V_{zz} is the largest component of the diagonalized EFG tensor, Q is the nuclear quadrupole moment, and h is Plank's constant.

The calculated values of σ_{iso}, C_Q, and η_Q for the different polymorphs are displayed in Table 6. The calculated σ_{iso} values for Al are scattered between 505.32 to 602.92 ppm, which cannot be compared directly with the experimental values because the calculated values correspond to absolute chemical shielding, whereas most experimental values are correspond to shifts relative to a known standard. However, one can compare experimental and theoretical values based on the relative shifts between different peaks. For example, in α' polymorphs, the Al1 and Al2 atoms are shifted 5 ppm relative to each other. For the γ phase, the shift between Al1 and Al2 is 27.56 ppm, which agrees very well with the experimentally reported value of 25.1 ppm.[52] Similarly, the C_Q and η_Q values are also scattered in wide range, and these values are directly comparable with experimental values.

Among the studied phases, the $hp1$ and γ phases have much higher quadrupolar coupling constant values. It should be noted that the NMR parameters are strongly related to the atomic environment (near neighbors) and quadrupolar coupling constants are directly related to the bond strength and anisotropy in the charge density distribution around the probe nuclei. For example, Al in the $hp1$ phase has high BOP value than that in the other polymorphs. Moreover, in $hp1$-phase, the Al is surrounded by nine H atoms and all these H atoms are shared by the next AlH_9 units (see Figure 1 in ref 10). Similarly, in the γ-phase, the octahedra are connected in such a way that they have a hydrogen-bridge bond formation surrounded by AlH_4 units. These are the possible reasons why the $hp1$ and γ-phases are having higher quadrupolar coupling constant values than the rest of the polymorphs.

From Table 6 it is evident that the calculated and experimentally observed C_Q and η_Q values for the α and γ phases are in good agreement with each other. In general, the theoretically predicted values are always lower than the experimental values for the C_Q and η_Q. It should be noted that present type of approach is not suitable for metallic systems (for more details, see ref 27). For the β, α', and $hp1$ phases, no experimental values are available for comparison. We hope that the present study will motivate experimentalists to investigate the NMR spectra for the other polymorphs of AlH_3.

In summary, the chemical bonding, NMR parameters, Raman- and IR-spectra, and lattice dynamical properties of different polymorphs of the AlH_3 have been studied by the first-principles method. Application of pressure makes sequence of phase transitions from $\beta \rightarrow \alpha' \rightarrow \alpha \rightarrow hp1\ (P63/m) \rightarrow hp2(Pm3\overline{n})$ and the estimated transition pressures are 2.4, 4.3, 64, and 104 GPa, respectively. Present theoretical prediction confirms that the previously identified high pressure polymorphs of AlH_3 are dynamically unstable at ambient condition and become stable at high pressures. The Born effective and Mulliken effective charge analyses reveal that the total charge of a H atom in these lattices is larger than 1.0 electron. The bond overlap population analysis indicates that the Al−H bonds are the strongest bonds in AlH_3 and the Al−H bonds in the $hp1$ phase are stronger than those in other polymorphs. The interactions between the H−H atoms are found to be very weak. The calculated charge density, Born effective, and Mulliken effective charges confirm that the chemical bonding character of AlH_3 polymorphs is predominantly ionic with noticeable covalent character (except in the $hp2$ phase). The $hp2$ phase has metallic character with mixed bonding behavior. The single crystal elastic constants and bulk modulus for the different polymorphs of the AlH_3 have been obtained. The computed compressibility values show that AlH_3 polymorphs are easily compressible. The calculated NMR parameters agree very well with the available experimental values for the α and γ phases.

■ ACKNOWLEDGMENT

The authors gratefully acknowledge the Research Council of Norway (Grant No: 460829, 185309/S30) and European Union seventh framework program under the "NanoHy" (Grant Agreement No.: 210092) project for financial support. P.V. gratefully acknowledges the Research Council of Norway for providing the computer time at the Norwegian supercomputer facilities.

■ REFERENCES

(1) Bogdanovic, B.; Schwickardi, M. *J. Alloys Compd.* **1997**, *253*−*25*, 1–9.

(2) Bogdanovic, B.; Brand, R. A.; Marjanovic, A.; Schwikardi, M.; Tölle, J. *J. Alloys Compd.* **2000**, *302*, 36–58.

(3) Brower, F. M.; Matzek, N. E.; Reigler, P. F.; Rinn, H. W.; Roberts, C. B.; Schmidt, D. L.; Snover, J. A.; Terada, K. *J. Am. Chem. Soc.* **1976**, *98*, 2450–2453.
(4) Schlapbach, L.; Züttel, A. *Nature* **2001**, *414*, 353–358.
(5) Turley, J. W.; Rinn, H. W. *Inorg. Chem.* **1969**, *8*, 18–22.
(6) Brinks, H. W.; Istad-Lem, A.; Hauback, B. C. *J. Phys. Chem. B* **2006**, *110*, 25833–25837.
(7) Brinks, H. W.; Langley, W.; Jensen, C. M.; Graetz, J.; Reilly, J. J.; Hauback, B. C. *J. Alloys Compd.* **2006**, *433*, 180–183.
(8) Yartys, V. A.; Denys, R. V.; Maehlen, J. P.; Frommen, C.; Fichtner, M.; Bulychev, B. M.; Emerich, H. *Inorg. Chem.* **2007**, *46*, 1051–1055.
(9) Ke, X.; Kuwabara, A.; Tanaka, I. *Phys. Rev. B* **2005**, *71*, 184107–184113.
(10) Vajeeston, P.; Ravindran, P.; Fjellvåg, H. *Chem. Mater.* **2008**, *20*, 5999–6002.
(11) Graetz, J.; Chaudhuri, S.; Lee, Y.; Vogt, T.; Muckerman, J. T.; Reilly, J. *Phys. Rev. B* **2006**, *74*, 214114–214121.
(12) Baranowski, B.; Hochheimer, H. D.; Strossner, K.; Honle, W. *J. Less-Common Met.* **1985**, *113*, 341–347.
(13) Goncharenko, I. N.; Glazkov, V. P.; Irodova, A. V.; Somenkov, V. A. *Phys. B* **1991**, *174*, 117–120.
(14) Scheicher, R. H.; Kim, D. Y.; Lebègue, S.; Arnaud, B.; Alouani, M.; Ahuja, R. *Appl. Phys. Lett.* **2008**, *92*, 201903.
(15) Kim, D. Y.; Scheicher, R. H.; Ahuja, R. *Phys. Rev. B* **2008**, *78*, 100102(R).
(16) Pickard, C. J.; Needs, R. J. *Phys. Rev. B* **2007**, *76*, 144114.
(17) Goncharenko, I.; Eremets, M. I.; Hanfland, M.; Tse, J. S.; Amboage, M.; Yao, Y; Trojan, I. A. *Phys. Rev. Lett.* **2008**, *100*, 045504.
(18) Aguayo, A.; Singh, D. J. *Phys. Rev. B* **2004**, *69*, 155103–155107.
(19) Wolverton, C.; Ozolins, V.; Asta, M. *Phys. Rev. B* **2004**, *69*, 144109–144125.
(20) Sandrock, G.; Reilly, J.; Graetz, J.; Zhou, W.-M.; Johnson, J.; Wegrzyn, J. *Appl. Phys. A: Mater. Sci. Process.* **2005**, *80*, 687–690.
(21) Blöchl, P. E. *Phys. Rev. B* **1994**, *50*, 17953–17979. Kresse, G.; Joubert, J. *Phys. Rev. B* **1999**, *59*, 1758–1775.
(22) Kresse, G.; Hafner, J. *Phys. Rev. B* **1993**, *47*, R558–561. Kresse, G.; Furthmuller, J. *Comput. Mater. Sci.* **1996**, *6*, 15–50.
(23) Perdew, J. P.; Burke, S.; Ernzerhof, M. *Phys. Rev. Lett.* **1996**, *77*, 3865–3868.
(24) Perdew, J. P.; Chevary, J. A.; Vosko, S. H.; Jackson, K. A.; Pederson, M. R.; Singh, D. J.; Fiolhais, C. *Phys. Rev. B* **1992**, *46*, 6671–6687.
(25) Parlinski, K.; Li, Z. Q.; Kawazoe, Y. *Phys. Rev. Lett.* **1997**, *78*, 4063–4066. **1998**, *81*, 3298.
(26) Refson, K.; Clark, S. J.; Tulip, P. R. *Phys. Rev.* **2006**, *B73*, 155114.
(27) Pickard, C. J.; F. Mauri, F *Phys. Rev.* **2001**, *B63*, 245101.
(28) Clark, S. J.; Segall, M. D.; Pickard, C. J.; Hasnip, P. J.; Probert, M. J.; Refson, K.; Payne, M. C. *Z. Kristallogr.* **2005**, *220*, 567–569.
(29) Perdew, J. P.; Burke, K.; Ernzerhof, M. *Phys. Rev. Lett.* **1996**, *77*, 3865–3868.
(30) King-Smith, R. D.; Vanderbilt, D. *Phys. Rev. B* **1992**, *47*, 1651–1654.
(31) Pick, R. M.; Cohen, M. H.; Martin, R. M. *Phys. Rev. B* **1970**, *1*, 910–920.
(32) Kunc, K.; Martin, R. *Phys. Rev. Lett.* **1982**, *48*, 406–409.
(33) Read, A. J.; Needs, R. J. *Phys. Rev. B* **1991**, *44*, 13071–13073.
(34) Gonze, X.; Charlier, J. C.; Allan, D. C.; Teter, M. P. *Phys. Rev. B* **1994**, *50*, 13035–13038.
(35) Zhong, W.; King-Smith, R. D.; Vanderbilt, D. *Phys. Rev. Lett.* **1994**, *72*, 3618–3621.
(36) Ravindran, P.; Vidya, R.; Kjekshus, A.; Fjellvåg, H.; Eriksson, O. *Phys. Rev. B* **2006**, *74*, 224412.
(37) Vajeeston, P.; Ravindran, P.; Kjekshus, A.; Fjellvåg, H. *Phys. Rev. B* **2005**, *71*, 216102(R).
(38) Brodsky, M. H.; Burstein, E. *J. Phys. Chem. Solids* **1967**, *28*, 1655–1668.
(39) Blat, D. K.; Zein, N. E.; Zinenko, V. I. *J. Phys.: Condens. Matter* **1991**, *3*, 5515–5524.
(40) Zogal, O. J.; Vajda, P.; Beuneu, F.; Pietraszko, A. *Eur. Phys. J. B* **1998**, *2*, 451–456.
(41) Tkacz, M.; Palasyuk, T.; Graetz, J.; Saxena, S. *J. Raman Spectrosc.* **2008**, *39*, 922–927.
(42) Mulliken, R. S. *J. Chem. Phys.* **1955**, *23*, 1833–1840.
(43) Ashcroft, N. W.; Mermin, N. D. *Solid State Physics*; Saunders College: Philadelphia, 1976.
(44) Nye, J. F. *Physical Properties of Crystals*; Clarendon: Oxford, 1957.
(45) Deyirmenjian, V. B.; Heine, V.; Payne, M. C.; Milman, V.; Lynden-Bell, R. M.; Finnis, M. W. *Phys. Rev. B* **1995**, *52*, 15191–15207.
(46) Hector, L. G.; Herbst, J. F.; Wolf, W.; Saxe, P. *Phys. Rev. B* **2007**, *76*, 014121.
(47) Marlo, M.; Milman, V. *Phys. Rev. B* **2000**, *62*, 2899–2907.
(48) Milman, V.; Warren, M. C. *J. Phys.: Condens. Matter* **2001**, *13*, 5585–5595.
(49) Karki, B. B.; Stixrude, L.; Clark, S. J.; Warren, M. C.; Ackland, G. J.; Crain *J. Am. Mineral.* **1997**, *82*, 635–638.
(50) Karki, B. B.; Clark, S. J.; Warren, M. C.; Hsueh, H. C.; Ackland, G. J.; Crain, J. *J. Phys.: Condens. Matter* **1997**, *9*, 375–380.
(51) Ravindran, P.; Fast, L.; Korzhavyi, P. A.; Johansson, B.; Wills, J.; and Eriksson, O. *J. Appl. Phys.* **1998**, *84* 4891.
(52) Hwang, S. J.; Bowman, R. C.; Grawtz, J.; Reilly, J. J. *Mater. Res. Soc. Proc.* **2006**, *927*, 0927–EE03-03.